PERGAMON

International Journal of Solids and Structures 40 (2003) 4461–4478

INTERNATIONAL JOURNAL OF SOLIDS and STRUCTURES

www.elsevier.com/locate/ijsolstr

The effects of thermal softening and heat conduction on the dynamic growth of voids

X.Y. Wu [a], K.T. Ramesh [a,*], T.W. Wright [a,b]

[a] *Department of Mechanical Engineering, The Johns Hopkins University, 122 Latrobe Hall 3400 N. Charles Street, Baltimore, MD 21218-2686, USA*

[b] *US Army Research Laboratory, Aberdeen Proving Ground, MD 21005, USA*

Received 14 November 2002

Abstract

This paper seeks to examine the dynamic growth of a single void in an elastic–plastic medium through analytical and numerical approaches. Particular attention is paid to the instability of void growth, and to the effects of inertia, thermal softening and heat conduction. A critical stress is known to exist for the unstable growth of voids. The dependence of this critical stress on material properties is examined, and this critical stress is demonstrated to correspond to the lower limit for the ductile spall strength in many materials. The effects of heat conduction on the dynamic growth of voids strongly depend on the time and length scales in the early stages of the dynamic void growth.

Keywords: Ductile failure; Dynamic; Plasticity; Instability

1. Introduction

The nucleation, growth and coalescence of voids is the principal mechanism in ductile fracture. Voids may be preexisting or may nucleate at second phase particles, and subsequently grow through plastic deformation of the surrounding matrix. The growth and interaction of a number of voids finally leads to void coalescence and ductile fracture. This paper examines the dynamic growth of voids under transient loading, with a specific focus on the coupled effects of thermal conduction and thermal softening.

A void in an infinite medium can grow without bound when the applied stress reaches a critical stress level. The existence of such an instability in nonlinear elastic solids was recognized by Ball (1982). Ashby et al. (1989) observed "cavitation instabilities" in tensile experiments on highly constrained ductile lead wires. Huang et al. (1991) addressed cavitation instabilities in elastic–plastic materials subjected to multiaxial axisymmetric loading and found that the condition for unstable void growth primarily depends on the

* Corresponding author. Tel.: +1-410-516-7735; fax: +1-410-516-7254.
E-mail address: ramesh@jhu.edu (K.T. Ramesh).

0020-7683/03/$ - see front matter © 2003 Elsevier Ltd. All rights reserved.
doi:10.1016/S0020-7683(03)00214-2

attainment of a critical value of the mean stress. Hereafter, we refer to this as the "critical stress." Note that this definition of the critical stress is independent of the loading history and rate sensitivity, and is different from the similarly named concept used by Tong and Ravichandran (1995) and Cortes (1992). Adopting the former definition of the critical stress, Wu et al. (2003) have addressed the effect of inertia in the problem of dynamic growth of a single spherical void (note that Tvergaard and Hutchinson (1993) showed that the initial void shape had little effect on the critical stress).

The problem of the dynamic growth of voids has been studied for many years, beginning with the work of Carroll and Holt (1972), who considered spherical voids in a finite rigid–plastic medium subjected to a hydrostatic loading using a spherical shell model. Johnson (1981) extended Carroll and Holt's model to a linear viscous material and found that the stabilizing effect of viscosity (rather than inertia) dominated the growth of voids in such a medium. Ortiz and Molinari (1992) considered the dynamic growth of a single spherical void in an infinite medium in a power-law hardening material. They showed that the effect of inertia is not significant until the void is larger than a characteristic dimension, but inertia tends to dominate long-term void growth. Wu et al. (2003) used the single spherical void model and adopted the concept of critical cavitation stress (Huang et al., 1991) to address the effects of inertia and rate-dependence on void growth. They found that, for a supercritical loading (i.e., an applied loading greater than the critical stress), all voids tend to achieve a constant rate of growth regardless of their initial sizes (so that voids with different initial sizes look similar in size after sufficient time). In addition, Wu et al. (2003) confirmed that rate sensitivity dominates the growth of voids at the early stage but gives way to the effect of inertia in the long-term. However, the combined effects of thermal softening and heat conduction were not taken into account; those combined effects are considered in this work.

Compared with the effects of rate sensitivity or strain hardening, the effect of thermal softening on void growth has drawn relatively little attention. Cortes (1992) used a spherical shell model to address strain hardening, rate sensitivity and thermal effects on dynamic void growth and concluded that the effect of thermal softening is weak compared to the effects of rate sensitivity and strain hardening (the effect of heat conduction was not included). Tong and Ravichandran (1993, 1995) incorporated thermal softening in both void collapse and void growth, and found that thermal softening accelerates the deformation process but is less important than the effect of strain hardening. It is obvious that these conclusions are appropriate for some specific materials. Cortes and Ellices (1993) also investigated cavitation instabilities in a shear band, where thermal softening dramatically lowers the critical stress. Heat conduction is not included in any of these studies.

This paper represents a continuation of the work begun in Wu et al. (2003), and focuses on the dynamic growth of voids with specific reference to instability, thermal effects and inertial effects and the consequences thereof in a variety of materials. The earlier paper considered the combined effects of rate-dependence and inertia, but did not include the effects of temperature or thermal conduction (except in the quasistatic case). The current paper addresses the fully coupled thermal and inertial case. A single spherical void model is used because this model helps us to separate the effects of temperature and inertia from the effect of void interactions, which enters into unit cell calculations through the outer boundaries (note that Zhang et al. (2002) show that the unit cell model is effectively equivalent to the single void model when the characteristic cell dimension is 10 times the void radius). We begin by examining several issues associated with instability of void growth, such as the effects of yield strain, strain hardening and thermal softening. The critical stresses are calculated for some ductile metals and alloys with consideration of those effects. Next, we address the length and time dependence of heat conduction in the problem of void growth. The conditions for the adiabatic and athermal growth of voids are obtained. Finally, numerical simulations are performed both in the non-inertial and inertial cases to investigate the influence of heat conduction on void growth. This influence is shown to be strongly affected by the initial void size and the applied loading rate.

2. General formulation

2.1. Material description

Consider an infinite medium containing a spherical void and subjected to a remote far-field hydrostatic loading as shown in Fig. 1. As the far-field loading p^{app} is increased, the surface of the void yields first, and then the elastic–plastic boundary (denoted by r_c) propagates outwards. The medium is assumed to be homogenous, isotropic and plastically incompressible. The matrix material surrounding the void is assumed to have strain hardening and thermal softening described by

$$\sigma_{\text{e}}/\sigma_{\text{Y}} = f(\varepsilon)\cdot h(T^*) \tag{1}$$

where σ_{Y} is the yield stress, ε the effective strain, T^* the temperature rise (room temperature is taken as the reference), and σ_{e} the effective stress, defined as $\sqrt{3/2 s_{ij}s_{ij}}$ where the s_{ij} are the components of the deviatoric stress tensor. In particular, the strain hardening function $f(\varepsilon)$ is assumed to represent power-law strain hardening, and the thermal softening function $h(T^*)$ is assumed to represent linear thermal softening:

$$\begin{aligned} &f(\varepsilon) = \varepsilon/\varepsilon_{\text{Y}} \quad \text{if } \varepsilon \leqslant \varepsilon_{\text{Y}} \\ &f(\varepsilon) = (\varepsilon/\varepsilon_{\text{Y}})^n \quad \text{if } \varepsilon \geqslant \varepsilon_{\text{Y}} \end{aligned} \tag{2}$$

$$h(T^*) = 1 - cT^* \tag{3}$$

where n is the strain hardening exponent, ε_{Y} the yield strain defined by σ_{Y}/E, E the Young's modulus, and c the coefficient of thermal softening. Once the temperature rise reaches $1/c$, the material completely loses load-carrying capacity. Linear thermal softening is usually justified because often heat conduction limits the growth of temperature, especially in small voids, as pointed out by Wu et al. (2003).

Since we are considering metals, a J_2 flow rule and normality are also applied

$$d_{ij}^{\text{p}} = \frac{3s_{ij}}{2\sigma_{\text{e}}}\dot{\varepsilon}^{\text{p}} \tag{4}$$

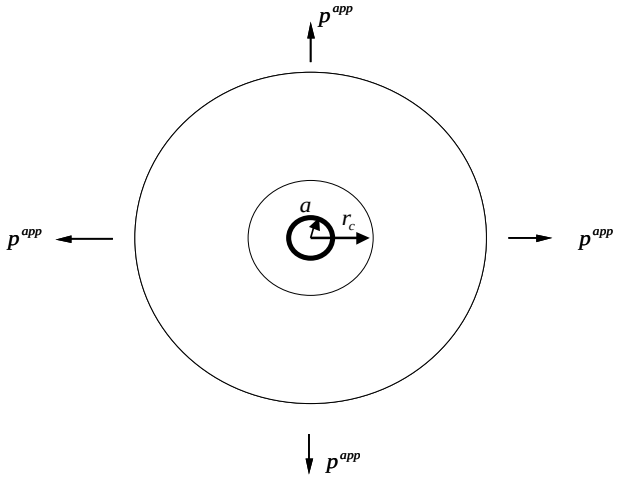

Fig. 1. Schematic diagram of the spherical single void model: an infinite body contains a single spherical void and is subjected to a remote hydrostatic tensile loading. After yield, the elastic–plastic boundary (denoted by its radius, r_c) propagates outwards and divides the whole region into two parts: the inner elastic–plastic region and the outer purely elastic region.

where

$$\dot{\varepsilon}^{\mathrm{p}} = \sqrt{(2/3)d_{ij}^{\mathrm{p}}d_{ij}^{\mathrm{p}}}, \qquad \varepsilon^{\mathrm{p}} = \int_0^t \dot{\varepsilon}^{\mathrm{p}}\,\mathrm{d}t. \tag{5}$$

Here d_{ij}^{p} is the plastic rate of deformation, $\dot{\varepsilon}^{\mathrm{p}}$ the effective plastic strain rate, and ε^{p} the effective plastic strain. The effects of strain rate were thoroughly covered in the previous paper (Wu et al., 2003), where it was shown that they primarily slow down the initial response to supercritical loading, and that eventually inertia dominates in the same way in every case. Thus this work focuses on the coupled thermal-inertial problem rather than the rate-dependent problem.

2.2. Kinematics

The problem described in Fig. 1 is essentially a 1D problem due to its geometry and the material properties. Accordingly, the deformation is described by

$$r = r(R, t) \tag{6}$$

where r and R are the radii in the current and undeformed configurations respectively. We use A to denote the initial void radius, and a to denote the current void radius. The effective strain has been proved to be the logarithmic strain and is,

$$\varepsilon = 2\ln(r/R). \tag{7}$$

If additional elastic deformation is neglected after yield, the effective plastic strain is then obtained as $\varepsilon^{\mathrm{p}} = \varepsilon - \varepsilon_{\mathrm{Y}}$. Plastic incompressibility requires

$$r^3 - R^3 = a^3 - A^3. \tag{8}$$

Once a void grows to a few times its initial size, $a^3 - A^3$ in Eq. (8) can be approximated as a^3. The incompressibility together with Eq. (7) then leads to

$$(a/r)^3 = 1 - \exp(-3\varepsilon/2). \tag{9}$$

The elastic–plastic boundary, denoted as r_c in Fig. 1, can be obtained by choosing ε as ε_{Y}. For $\varepsilon_{\mathrm{Y}} = 0.002$ (a typical value for metals), the plastic zone will be about seven times the current void size. Eq. (9) shows that the effective strain decays rapidly away from the void surface (e.g. $\varepsilon \approx 1$ at $r = 1.09a$, while $\varepsilon \approx 0.2$ at $r = 1.65a$).

2.3. Conservation of energy in the adiabatic case

During the dynamic growth of voids, the local temperature increases because of the plastic work being dissipated as heat. If heat conduction is included, for a spherically symmetric problem, the conservation of energy requires

$$\rho c_{\mathrm{p}} \frac{\mathrm{d}T^*}{\mathrm{d}t} = \frac{k}{r^2}\frac{\partial}{\partial r}\left(r^2\frac{\partial T^*}{\partial r}\right) + \eta\sigma_{\mathrm{e}}\cdot\dot{\varepsilon}^{\mathrm{p}}. \tag{10}$$

Here k is the thermal conductivity of the material, ρ is the density, c_{p} is the specific heat at constant pressure, and η is the fraction of plastic work transformed into heat (assumed to be 0.9 in our case). A local temperature rise in the adiabatic condition is described by

$$\rho c_{\mathrm{p}}\mathrm{d}T = \eta\sigma_{\mathrm{e}}\mathrm{d}\varepsilon^{\mathrm{p}} \tag{11}$$

Here, for linear thermal softening, $h(T^*)$ can be related explicitly to the strain by substituting (1)–(3) into (11):

$$h(T^*) = \exp\left\{ -\frac{c\eta\sigma_Y}{(n+1)\rho c_p} \cdot (\varepsilon \cdot f(\varepsilon) - \varepsilon_Y) \right\}. \tag{12}$$

Eq. (12) indicates that the magnitude of thermal softening (measured by $h(T^*)$) depends on the combination of material properties $c\sigma_Y/((n+1)\rho c_p)$ (computed for some metals and alloys in Table 1), the strain ε, and the strain hardening factor $f(\varepsilon)$ (when the effective strain is large, ε_Y may be neglected in comparison). The temperature rise can be calculated explicitly from Eq. (12) in this adiabatic case. It is possible that the temperature rise is very high on the void surface where large plastic deformations occur. However, the temperature rise cannot exceed $1/c$, since at that point the material will completely lose its load-carrying capacity (Eq. (3)). The plastic deformation is localized, and therefore so is the effect of thermal softening, since the thermal softening function is an exponential function of ε (note that $f(\varepsilon) > 1$).

3. Analysis and results

In this section, we first examine the critical stresses for unstable growth of voids both in the non-thermal (''athermal'') and adiabatic cases. Specific values of the critical stress are calculated for several metals and alloys. Next, we discuss the size-dependence introduced by the effect of heat conduction. Lastly, we introduce the effect of inertia into the growth of voids. The combined effects of inertia, thermal softening and heat conduction are examined using numerical simulations.

3.1. Cavitation instability

The equilibrium equation in spherical coordinates is

$$\frac{\partial\sigma_r}{\partial r} - \frac{2\sigma_e}{r} = 0, \tag{13}$$

where σ_r is the radial stress. The assumed loading history is that shown in Fig. 2: a remote loading is developed at a constant rate q to a given level p_s over a rise time t_R, and is then held for a time t_h. The void surface is traction free, and a dead-load boundary is applied at infinity ($\sigma_r = p^{app}$). The critical stress for unstable growth of the void is obtained (Wu et al., 2003) by integrating Eq. (13):

$$p_c = \frac{2}{3}\sigma_Y + \int_{\varepsilon_Y}^{\infty} \frac{\sigma_e}{\exp(3\varepsilon/2) - 1}\, d\varepsilon. \tag{14}$$

When the applied loading reaches p_c, the void will grow without bound (Wu et al., 2003). Eq. (14) shows that the outer elastic region contributes $2/3\sigma_Y$ to the critical stress, and that the contribution from the plastic zone depends on the plastic behavior through the effective stress σ_e and on the size of the plastic zone through the lower limit of the integral, ε_Y. For the power-law strain hardening and linear thermal softening material described in Eqs. (1)–(3), we focus on the dependence of the critical stress on the following parameters: the strain hardening exponent n, the thermal softening coefficient c and the nominal yield strain ε_Y. We consider both the non-thermal and adiabatic cases (in the latter case, the effect of thermal softening is included).

Beginning with the non-thermal condition, Fig. 3 presents the computed critical stress (normalized by the yield stress) as a function of the nominal yield strain ε_Y for a range of strain hardening exponents n (a table showing this dependence is presented by Huang et al. (1991)). The normalized critical stresses decrease rapidly once the yield strain increases to 0.1%. The critical stress is relatively insensitive to the yield strain in

Table 1
Material properties and several property groups used in the computations for a selected set of metals and alloys. Computed (non-thermal/adiabatic) critical stresses are presented, as are measured spall strengths for several of these materials

Material	Yield stress σ_Y (MPa)	Specific heat c_p (J/kg K)	Thermal conductivity k (W/m K)	Mass density ρ (g/cm^3)	$k/\rho c_p$ 10^{-6} m^2/s	Strain hardening exponent n	Thermal coefficient c (10^{-3} K^{-1})	$\frac{c\sigma_Y}{(n+1)\rho c_p}$	Melting temperature T_m (°C)	Calculated yield strain ε_Y (%)	Critical stress (GPa)	Spall strength (GPa)
Aluminum	10	900	247	2.699	102	0.28	3	0.02	660.4	0.013	0.31/0.3	0.5–1.1[a]
Cu (annealed)	33	386	398	8.93	115	0.34	2	0.05	1084	0.024	1.07/0.94	0.6–2.3[a]
Cu (cold drawn)	333	386	398	8.93	115	0.007	2	0.48	1084	0.24	1.53/1.43	
Iron	69	456	80	7.87	22	0.33	1.25	0.02	1538	0.026	2.03/1.89	
α-Titanium[b]	337	522	17	4.6	7	0.1	1	0.14	1668	0.25	1.95/1.87	2.2–3.7[a]
Tantalum	700[c]	139	54	16.6	24	0.17	0.5	0.13	2996	0.34	4.2/3.93	4.4–6.8[c]
6061-T6 Al	276	896	167	2.7	69	0.024	2	0.23	582	0.35	1.22/1.18	1.2–2.0[c]
7075-T6 Al	505	960	130	2.81	48	0.03	2	0.37	532	0.63	2.04/1.91	
2024-T4 Al[d]	325	875	120	2.78	49	0.08	2	0.25	502	0.39	1.61/1.51	1.25[a]
Mild steel[e]	220	482	60	7.9	16	0.15	1	0.06	1492	0.092	1.91/1.86	
4340 Steel[d]	1480	475	45	7.85	12	0.02	1	0.4	1750[e]	0.61	5.88/5.5	5.3[a]
Maraging steel[d]	1760	480	25	8	6.6	0.01	1	0.45		0.8	6.5/5.89	
Ti–6Al–4V[d]	880	526	6.7	4.43	2.9	0.02	1	0.34	1660	0.67	3.8/3.56	4.1–5.0[c]

All data from ASM handbooks except:
[a] Davison and Graham (1979).
[b] Data from Chichili (1998).
[c] Grady (1988).
[d] Data from www.matweb.com
[e] Data from Ashby and Jones (1998a,b).

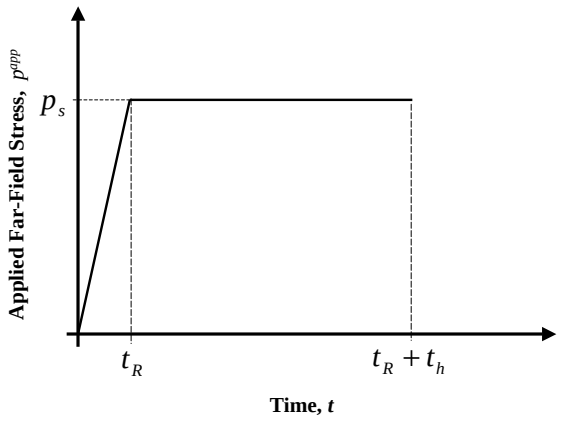

Fig. 2. History of applied far-field loading. Initially the load increases at a constant loading rate until the end of the rise-time t_R, and is then held steady at magnitude p_S for an additional time t_h.

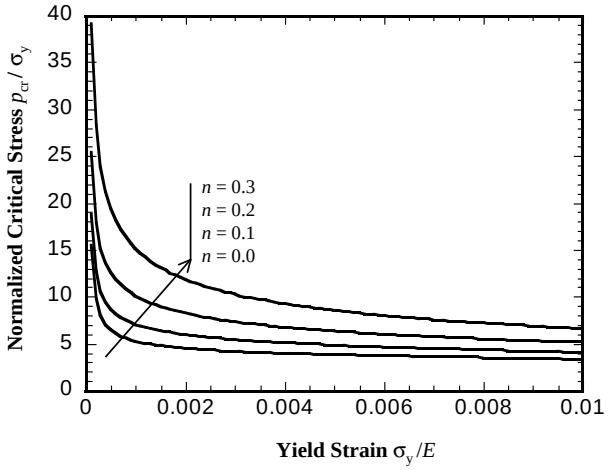

Fig. 3. Variation of the non-thermal critical stress (normalized by the yield stress) with yield strain for various strain hardening exponents (quasistatic calculation). The yield strain has a strong influence on the critical stress at high strain hardening and at low yield strains.

the range of yield strain from 0.2% to 1% (appropriate for most metallic alloys). Note that the dependence of the critical stress on the yield strain is strongly coupled with the effect of strain hardening in this non-thermal case. At high strain hardening, the yield strain has a stronger influence on the critical stress. From a materials perspective, relatively pure metals have low yield strengths and therefore low yield strains, while they typically have high strain hardening. Thus, the influence of yield strain on the critical stress is significant for pure metals. When metals are alloyed to increase their yield strengths and therefore yield strains, there is also normally a reduction of the strain hardening that can be developed, so that the influence of yield strain on the critical stress is likely to be relatively unimportant for most heavily alloyed metals. The yield strain may also be very small in the cases of annealed materials with very high moduli.

Direct measurements of the critical stress are rarely reported. An early work by Gent and Lindley (1958) shows that the critical stress for cavitation reaches half of Young's modulus in rubber, which has no apparent yield stress, but this cannot easily be described in the current model. Ashby et al. (1989) measured the critical stress in lead with $n = 0.25$, and obtained a value of 5–$7\sigma_Y$. Our computed value for this case is $8\sigma_Y$, but we are considering purely hydrostatic states (Huang et al. (1991) provide a detailed comparison with that experiment). Note, however, that a pure power-law strain hardening response as used in Eq. (2) usually overestimates the effective stress at low strains.

Considering now both the non-thermal and adiabatic cases, the coupled effects of strain hardening, yield strain and thermal softening on the critical stress are computed for some ductile metals and alloys. The assumed power-law strain hardening and linear thermal softening functions are used to fit the actual, more complex thermo-mechanical responses of these materials presented in the literature. Table 1 collects together the material properties and several property groups used in the computations. The strain-hardening exponents are calculated from $\sigma_f/\sigma_Y = (\ln \delta/\varepsilon_Y)^n$, where δ is the elongation at which the ultimate strength σ_f is achieved. The thermal softening coefficient, $1/T_m \leqslant c \leqslant 2/T_m$, is estimated from handbook data. Using these material properties, the critical stresses are then computed for each material using Eq. (14), and these are presented for both the non-thermal (open triangle) and the adiabatic (solid triangle) conditions in Figs. 4 (normalized data) and 5 (absolute values). It is important to recognize that the yield strengths, strain hardening rates and thermal softening rates of these metals are strongly influenced by impurity content, heat-treatment condition and prior plastic work, so that the critical stresses for these materials may vary considerably for structural materials in service.

Fig. 4 presents the normalized critical stresses for those materials shown in Table 1. The critical stresses are around $4\sigma_Y$ for most of the alloys (6061 Al, 7075 Al, 4340 steel, maraging steel, Ti–6Al–4V)—note that these have little strain hardening but moderate yield strains ($0.002 < \varepsilon_Y < 0.01$). The critical stresses vary from $5\sigma_Y$ to $10\sigma_Y$ for the materials with moderate strain hardening and moderate yield strains, such as tantalum, titanium, α-titanium and mild steel. However, for pure metals with strong strain hardening but extremely low yield strains (i.e. iron, annealed copper and aluminum), the normalized critical stresses are very high (around $30\sigma_Y$). The adiabatic critical stresses are generally 5–12% lower than the non-thermal critical stresses, showing the impact of the thermal softening (most apparent in this figure for the pure

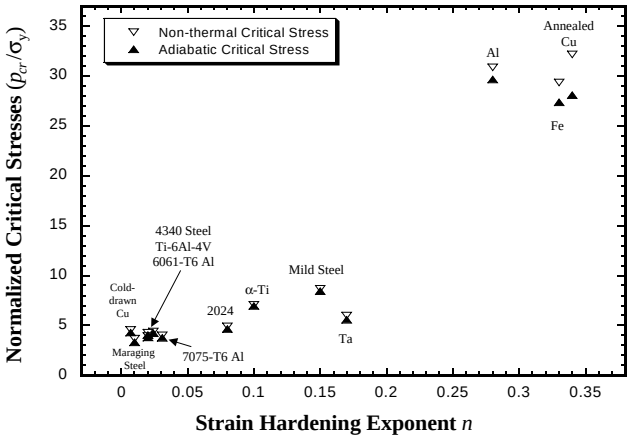

Fig. 4. Normalized critical stresses (normalized by the yield stress) for the materials in Table 1, plotted against the strain hardening exponent. Both non-thermal (open triangle) and adiabatic (solid triangle) critical stresses are presented. The normalized critical stresses vary from 4 to 10 for most alloys, but for some pure metals they can reach 30. The adiabatic critical stress is typically 5–12% less than the non-thermal critical stress, indicating the importance of thermal softening.

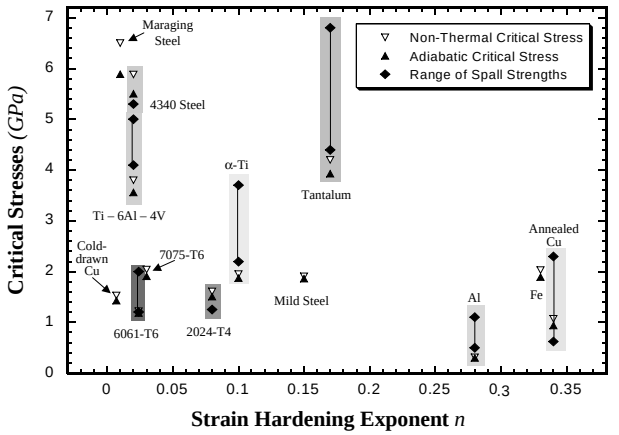

Fig. 5. The absolute values of the computed non-thermal (open triangle) and adiabatic (solid triangle) critical stresses for the materials in Table 1. Note that the absolute critical stress levels are 1–3 GPa for most of these materials, although they can be much higher for extremely high strength alloys (4340 steel and maraging steels). The figure also presents measured values of the spall strength for some of these materials from the literature (the range of measured data is represented by a line bounded by the diamonds). Results for each material are collected together in the shaded rectangles where appropriate. Note the strong correlation between the measured incipient spall strengths and the computed critical stresses.

metals). Applied loadings that are greater than the adiabatic critical stress but less than the non-thermal critical stress are referred to henceforth as ''intermediate'' loadings. One consequence of the separation of the critical stresses induced by thermal softening is that intermediate loadings will result in interesting phenomena tied to thermal conduction.

The absolute values of the computed adiabatic and non-thermal critical stresses are presented in Fig. 5. For most of the materials listed in Table 1, the critical stresses fall in the range of 1–3 GPa, even though the yield stresses, the yield strains and the strain-hardening exponents vary significantly from one material to another. For example, annealed copper and cold drawn copper have significant differences in their yield stresses and strain hardening and so very different normalized critical stresses (Fig. 4), but the absolute values for their critical stresses are quite similar. Tantalum is computed to have relatively high critical stresses for a pure metal because of its high yield strength at room temperature. Very high critical stresses (in the range of 6–7 GPa) are computed for maraging steels and 4340 steels, due to their extremely high yield stresses; the influence of the thermal softening also appears to be greatest for these materials. The lowest critical stresses are computed for pure aluminum at 300 MPa. Measurements of the critical stresses of these materials are not available, and so direct comparison with experimental data is not possible in Fig. 5. However, we may compare the computed critical stresses with observations of the spall strength of these materials; that comparison is discussed in a later section.

3.2. The influence of heat conduction

The effect of heat conduction has not been considered in the results presented to this point. In this section, we focus on the size dependence introduced by heat conduction in the void growth problem, and begin by scaling the equation of energy conservation in the diffusive case. The analyses are applicable to the growth of voids both in the non-inertial case (discussed to this point) and the inertial case, which remains to be examined in the next section.

Eq. (10) presented the energy equation for this spherically symmetric problem including heat conduction. A scaling law is used to address the length dependence of heat conduction. The dimensionless temperature

rise $\widetilde{T}$, dimensionless radius $\tilde{r}$, dimensionless strain rate $\tilde{\dot{\varepsilon}}^{\mathrm{p}}$, and dimensionless effective stress $\tilde{\sigma}_{\mathrm{e}}$ are defined as

$$\tilde{T}^* = T^* \cdot c, \qquad \tilde{r} = r/a, \qquad \tilde{\dot{\varepsilon}}^{\mathrm{p}} = \dot{\varepsilon}^{\mathrm{p}}/\dot{\varepsilon}_0, \qquad \tilde{\sigma}_{\mathrm{e}} = \sigma_{\mathrm{e}}/\sigma_{\mathrm{Y}} \tag{15}$$

where $\dot{\varepsilon}_0 = 2\dot{a}/a$ is the strain rate on the surface of the void. Eq. (10) can now be rewritten in terms of the scaled quantities as

$$\frac{\rho c_{\mathrm{p}}}{c} \cdot \frac{\mathrm{d}\tilde{T}^*}{\mathrm{d}t} = \frac{k}{a^2 c} \cdot \frac{1}{\tilde{r}^2} \frac{\partial}{\partial \tilde{r}} \left(\tilde{r}^2 \frac{\partial \tilde{T}^*}{\partial \tilde{r}} \right) + \frac{2\eta \sigma_{\mathrm{Y}} \dot{a}}{a} \cdot \tilde{\sigma}_{\mathrm{e}} \cdot \tilde{\dot{\varepsilon}}^{\mathrm{p}} \tag{16}$$

The left side of Eq. (16) represents the rate (per unit volume per unit time) of the energy needed to increase the temperature. On the right side, the first term represents the rate of heat conduction, and the second term the rate of plastic work transformed into heat. Plastic work is only done in the plastic zone, the size of which is $r_c = (2/3\varepsilon_{\mathrm{Y}})^{1/3} a$ (hence the use of a to normalize r in Eq. (16)). The rate of plastic work done is very high in the localized region near the surface of the void. Therefore, the potential temperature rise is also very high. Heat conduction moves the heat generated away from the inner hot region into the (larger) exterior cooler region. If the heat is conducted away sufficiently quickly, the temperature in the matrix material will be uniformly low, and the void growth will be essentially non-thermal. In contrast, if the heat cannot be conducted away sufficiently quickly, the temperature in the matrix near the void will build up and the void growth will be nearly adiabatic. Thus, the efficiency of heat conduction determines whether a void will grow non-thermally or adiabatically.

A measure of the influence of heat conduction may be obtained by comparing the characteristic length associated with thermal diffusion with the length scale associated with the plastic zone (since this is where heat is generated). The characteristic length associated with thermal diffusion is typically defined as $h_{\mathrm{diff}} = 2\sqrt{k\tau/\rho c_{\mathrm{p}}}$, and represents the distance effected by thermal diffusion over the time interval τ. In our case we may usefully choose $\tau = a/2\dot{a}$ (the reciprocal of the strain rate at the void surface). Thus the characteristic length associated with thermal diffusion is $h_{\mathrm{diff}} = \sqrt{2ka/\rho c_{\mathrm{p}} \dot{a}}$. The comparative length scale is that associated with the plastic zone, and the radius of the plastic zone is $r_c = (2/3\varepsilon_{\mathrm{Y}})^{1/3} a$. Considering the ratio of these two length scales, we define simple criteria to determine when the adiabatic void growth or the non-thermal void growth idealizations are reasonable:

$$\begin{aligned} &a\dot{a}/\Omega < 0.01 \text{ for non-thermal growth} \\ &a\dot{a}/\Omega > 100 \text{ for adiabatic growth} \end{aligned} \tag{17}$$

where $\Omega = 2.6k/\rho c_{\mathrm{p}} \varepsilon_{\mathrm{Y}}^{2/3}$ is a combination of material properties. We have used the results of numerical simulations (such as those presented here and in Wu et al., 2003) to estimate the numbers on the right hand sides of conditions (17). Note that the influence of heat conduction on void growth is strongly affected by the current void size and the rate of void growth, because of the length scale and the time scale introduced by the thermal diffusion. Eq. (17) indicates that a small void is more likely to grow non-thermally, and a big void is more likely to grow adiabatically.

In the non-inertial case, the rate of void growth may be directly related to the loading rate. Once yield has occurred at the void surface, the equilibrium Eq. (13) can be integrated:

$$p^{\mathrm{app}} = \frac{2}{3}\sigma_{\mathrm{Y}} + \int_{\varepsilon_{\mathrm{Y}}}^{2\ln(a/A)} \frac{\sigma_{\mathrm{e}}}{\exp(3\varepsilon/2) - 1}\, \mathrm{d}\varepsilon. \tag{18}$$

Henceforth, we use ε_a to denote $2\ln(a/A)$ (the strain on the surface of the void), and use Λ to denote $\int_{\varepsilon_{\mathrm{Y}}}^{2\ln(a/A)} \sigma_{\mathrm{e}}/(\exp(3\varepsilon/2) - 1)\, \mathrm{d}\varepsilon$. In the non-thermal case, the effective stress σ_{e} is a power-law function of strain ε. In the adiabatic case, the effective stress σ_{e} can be expressed in terms of strain ε using the adiabatic stress-strain relationship. Thus, in both cases Λ is a monotonic function of ε_a, so that $\Lambda = \Lambda(\varepsilon_a)$. Thus, for

both the non-thermal and adiabatic cases, one may relate the rate of void growth $\dot{a}$ to the rate of loading q by taking the time-derivative of Eq. (18):

$$q = \Lambda'(\varepsilon_a) \cdot 2\dot{a}/a \tag{19}$$

where $\Lambda'(\varepsilon_a) = \frac{d\Lambda}{d\varepsilon}$ at $\varepsilon = \varepsilon_a$. The loading history remains the same as that described in Fig. 2, so that a constant loading rate q holds for the rise time t_R.

In the diffusive case, however, the effective stress σ_e depends not only on the strain ε but also on the history of deformation. Therefore, Λ is deformation-history dependent rather than a monotonic function of ε_a. However, for a given loading condition and a given initial void size we can still define the value of $\Lambda'(\varepsilon_a)$ at $\varepsilon = \varepsilon_a$, so that Eq. (19) can be applied to the thermally diffusive case. Using Eq. (19) and conditions (17), we obtain modified conditions for the adiabatic and athermal growth of voids in this non-inertial case with constant applied loading rate q:

$$\begin{aligned} &qa^2/2\Lambda'(\varepsilon_a)\Omega < 0.01 \text{ for non-thermal growth,} \\ &qa^2/2\Lambda'(\varepsilon_a)\Omega > 100 \text{ for adiabatic growth.} \end{aligned} \tag{20}$$

Note that the influence of heat conduction on void growth is strongly affected by the current void size as well as the applied loading rate for the non-inertial case. Thus at high loading rates, void growth tends to be adiabatic. The influence of heat conduction on void growth changes as the void grows, both because of the change in the void size and because of the change in $\Lambda'(\varepsilon_a)$ in conditions (20). Assuming a constant rate of applied load, $\Lambda'(\varepsilon_a)$ decreases as the void grows. In the thermally diffusive case Λ is no longer a monotonic function of ε_a, and if the applied loading is sufficiently high, $\Lambda'(\varepsilon_a)$ could be zero (implying instability) or even negative (implying that the equilibrium condition is no longer valid). Condition (20) shows that unstable void growth will be essentially adiabatic in the non-inertial case.

We have performed numerical simulations to further explore these effects of thermal diffusion on void growth (at this stage, without considering inertia). The results are presented here for one particular material, a maraging steel with the properties corresponding to that in Table 1. The applied loading history is that described in Fig. 2, with $q = 10$ GPa/μs and a rise time of 640 ns. The saturation level of the applied loading is chosen to be an intermediate value of $3.6\sigma_Y$, between the non-thermal ($3.7\sigma_Y$) and adiabatic ($3.4\sigma_Y$) critical loadings, so that the influence of heat conduction on the void growth can be most easily demonstrated (the results for subcritical loading—below the adiabatic critical stress—can be deduced from the work of Wu et al., 2003). Varying initial void sizes are considered, and the relative growth of the voids (normalized by the initial void size) is plotted against time for the non-thermal, adiabatic and diffusive cases in Fig. 6.

In the non-thermal case, each void expands at a steadily increasing rate while the applied loading increases, but stops when the applied load is held steady (since this saturation level is below the non-thermal critical stress). In the adiabatic condition, the early void growth is similar to the non-thermal response, but then becomes more rapid, and eventually unstable growth occurs when the applied load reaches the adiabatic critical stress (at around 600 ns in this particular case). Note that in the non-thermal and adiabatic cases, the initial void size is irrelevant so that the void growth looks the same for the full range of void sizes. In contrast, the diffusive growth of the voids shows strong size dependence. Results are presented in Fig. 6 for five different initial void sizes: 10, 1, 0.1, 0.02 and 0.01 μm. The growth (with diffusion) of the 10 μm void is very close to that observed in the adiabatic case, while the growth (with diffusion) of the 0.01 μm void is very similar to that observed in the non-thermal case (because the heat generated by the plastic work is being conducted away sufficiently rapidly). This illustrates the two limiting idealizations described in conditions (20). When one considers an intermediate initial void size such as the 1 μm case, the growth is initially slower than the adiabatic response (because of thermal diffusion) but eventually catches up with the adiabatic growth curve when the applied load approaches the adiabatic critical stress. The void growth in

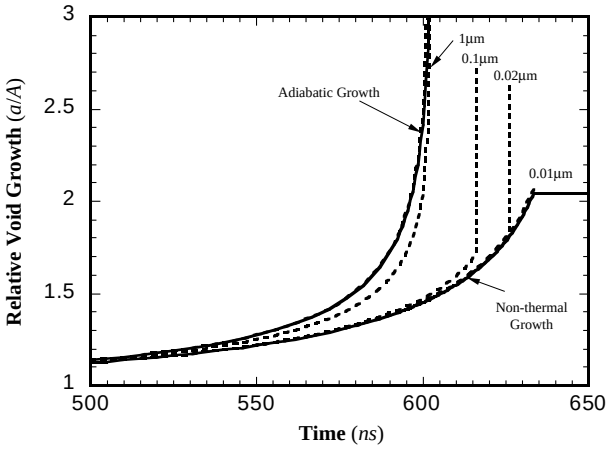

Fig. 6. Quasistatic void growth as a function of time in the adiabatic (solid line), non-thermal (solid line) and diffusive (dashed lines) cases (with initial void sizes of 10, 1, 0.1, 0.02 and 0.01 μm). The material properties correspond to the maraging steel in Table 1. The applied loading history is that described in Fig. 2, with $q = 10$ GPa μs, a rise time t_R of 640 ns. The saturation level of the applied loading is chosen to be an intermediate value of $3.6\sigma_Y$, between the non-thermal ($3.7\sigma_Y$) and adiabatic ($3.4\sigma_Y$) critical loadings.

the 0.02 and 0.1 μm cases is similar to the non-thermal growth for much of the time but eventually becomes unstable (once $\Lambda'(\varepsilon_a)$ becomes zero). For both of these void sizes, this instability occurs well after the applied load has passed the adiabatic critical stress (the instability occurs earlier for the larger void). This is of course because the heat is being conducted away in these diffusive cases, reducing the destabilizing effects of thermal softening and delaying the onset of the instability. The case of the 0.01 μm void shown in Fig. 6 demonstrates that if the saturation level of the applied loading is held at a value below the non-thermal critical stress, the growth of some small voids will stop. That is, heat conduction terminates the growth of sufficiently small voids for intermediate loadings.

One would expect that the influence of heat conduction on void growth is also affected by the loading rate. Understanding this interaction requires an examination of the combined effects of inertia, thermal softening and heat conduction on void growth, and this is discussed in the next section.

3.3. Dynamic growth, heat conduction and thermal softening

In spherical coordinates, the equation of motion is

$$\frac{\partial \sigma_r}{\partial r} - \frac{2\sigma_e}{r} = \rho \ddot{r}. \tag{21}$$

The velocity and acceleration of particles can be determined in terms of the velocity and acceleration at the void surface ($r = a$) from the incompressibility of the material:

$$\dot{r} = \frac{a^2}{r^2}\dot{a}, \qquad \ddot{r} = -\frac{\partial}{\partial r}\left(\frac{a^2\ddot{a}}{r} + \frac{2a\dot{a}^2}{r} - \frac{a^4\dot{a}^2}{2r^4}\right). \tag{22}$$

Using (22) to integrate (21), we obtain for this inertial case (see Wu et al., 2003):

$$\frac{\rho(a\ddot{a} + 3\dot{a}^2/2)}{\sigma_Y} = \frac{p^{app}}{\sigma_Y} - \int_0^{2\ln(a/A)} \frac{\sigma_e/\sigma_Y}{\exp(3\varepsilon/2) - 1}\, d\varepsilon. \tag{23}$$

Under a supercritical loading, the integral on the right will saturate at large strain and a constant rate of void growth (termed an "equilibrium rate" $\dot{a}_e$) will be achieved (Wu et al., 2003):

$$\dot{a}_e = \sqrt{2(p^{app} - p_{cr})/3\rho}. \tag{24}$$

The term in parentheses above is referred to as the degree of supercriticality. The magnitude of the equilibrium rate depends on the mass density and the degree of supercriticality, and therefore may depend quite strongly on thermal effects. Consider, for example, an applied loading that is 10% higher than the non-thermal critical stress. Suppose further that the non-thermal critical stress itself is 10% higher than the adiabatic critical stress (a likely situation, given the results in Fig. 4). Then, Eq. (24) shows that the equilibrium rate of void growth achieved in an adiabatic problem will be 1.4 times the equilibrium rate achieved in the non-thermal problem. Thus, thermal softening may result in a substantial increase of the rate of void growth under supercritical loading, even though it has a relatively small effect on the critical stress.

Another important aspect of the equilibrium rate $\dot{a}_e$ is that it is independent of the initial void size, so that voids of all sizes will attain the same growth rate in the long term for supercritical loading. This phenomenon is explored in detail by Wu et al. (2003).

Numerical simulations have been performed to scrutinize these interesting thermal coupling issues in the inertial case. We first simulate the dynamic growth of voids in the same material (maraging steel) with the same intermediate loading condition (i.e., we repeat the simulations performed for Fig. 6, but this time we incorporate inertia and solve the equation of motion rather than the equilibrium equation). Once again we consider a range of initial void sizes (10, 1, 0.1, 0.03 and 0.01 μm), so that we may explore coupled inertial and thermal effects (note that the purely inertial case has been explored previously by Wu et al. (2003)). Fig. 7 presents the dynamic growth of the voids with both thermal softening and heat conduction incorporated in the calculation: the current void size is plotted as a function of time for the full range of initial void sizes (note this is a semi-logarithmic plot). The void that was initially 0.03 μm in diameter nearly catches up with the void that was initially 0.1 μm within a few tens of nanoseconds; both of these catch up with the void that was initially 1 μm in about 200 ns, and in a microsecond all three of these voids are almost as big as the void that was initially 10 μm. This behavior is a consequence of the independence of $\dot{a}_e$ on the initial void size described previously (Wu et al., 2003). The new result here that arises from the coupling of the thermal and inertial effects is that observed for the void that was initially 0.01 μm: this void stops growing once the load reaches its saturation value, because the heat is being conducted away sufficiently quickly. Thus, heat

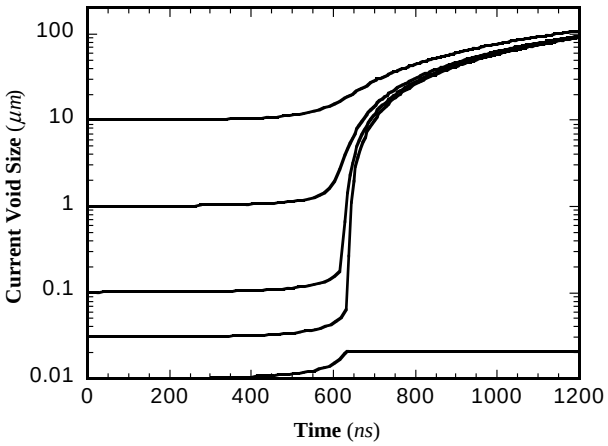

Fig. 7. Dynamic void growth under the same applied loading as in Fig. 6 (note this is a semi-logarithmic plot). A range of initial void sizes (10, 1, 0.1, 0.03 and 0.01 μm) is considered, and thermal diffusion is included. Note how the smaller voids appear to catch up with the larger voids, except the smallest void which stops growing as a result of heat conduction.

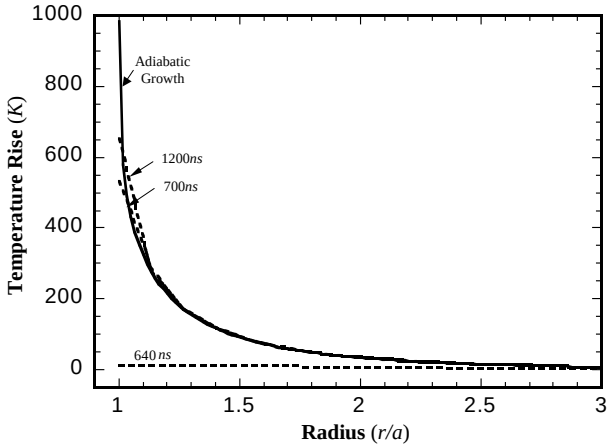

Fig. 8. Radial distributions of temperature at various times for the 0.03 μm void (corresponding to the diffusive computations presented in Fig. 7). For purposes of comparison, the radial temperature distribution that is obtained from a purely adiabatic calculation (at a time of 700 ns, by which time the temperature rise has reached $1/c$ at the void surface) is presented as the solid line.

conduction effectively sets a cut-off size in this problem. Voids with initial sizes smaller than the cut-off size will stop growing eventually, while voids with initial sizes bigger than the cut-off size continue to grow rapidly and quickly become similar in size as a result of the equilibrium rate of growth.

The radial distribution of temperature is shown in Fig. 8 at various times for the 0.03 μm void (corresponding to the diffusive computations presented in Fig. 7). For purposes of comparison, we also present the radial temperature distribution that is obtained from a purely adiabatic calculation (at a time of 700 ns, by which time the temperature rise has reached $1/c$ at the void surface). Note that the rise time of the loading is $t_R = 640$ ns. In the diffusive case, there is no apparent temperature rise at the end of the rise time for this void size. Just 60 ns later (at 700 ns), the temperature at the void surface has built up considerably, and the temperature profile is beginning to approach that in the adiabatic calculation, and at 1200 ns the temperature profile is even closer to the adiabatic result. These computed temperature profiles are consistent with our earlier analyses, since comparison with Fig. 7 shows that at these later times the void is growing extremely rapidly as a result of the supercritical loading.

The relative effects of thermal conduction and inertia on void growth can be described as follows. Both induce size dependence. However, thermal conduction becomes extremely important for very small voids, resulting in a stabilizing influence by removing heat from the vicinity and leading to athermal growth. The influence of thermal conduction is relatively unimportant for large voids, which tend to grow in near-adiabatic fashion (depending on the loading rate, of course). In contrast, inertia is particularly important for large voids and relatively unimportant for small voids (see Wu et al., 2003 for a discussion of this effect). Thus each of these effects is important in different regimes of void size.

4. Discussion

4.1. Comparison with incipient spall strength

Spallation is a dynamic material failure produced by the action of tensile stresses developed in the interior of a body as a result of wave loading Davison and Graham (1979). A common experimental

technique for investigating spallation is through the normal impact of flat plates (Davison and Graham, 1979; Meyers, 1994) to generate shock loading. Laser-based shock loading techniques (Dekel et al., 1998; Moshe et al., 1998, 2000) have also become available. Typically these techniques generate stress pulses with very high amplitudes (several GPa) with durations that range from a few nanoseconds (particularly in the laser-based shock techniques) to a microsecond or so. When a plane wave is reflected from the rear surface of a sample and returns towards the impact surface, the tensile stress reaches a maximum at a "spall zone," where the rarefaction wave reflected from the free surface collides with a second rarefaction wave propagating from the impact surface. If the magnitude and duration of this tensile stress exceeds a threshold stress level (commonly called the spall strength), spallation can take place through the nucleation, growth and coalescence of voids (ductile spall) or cracks (brittle spall). The spall strength of the material can then be obtained through measurement of the free surface velocity (the so-called pull-back velocity) (Speight and Taylor, 1986); we will use this definition of spall strength for purposes of discussion. More formally, we will use an operational definition: the "incipient spall strength" in ductile materials is defined (Chevrier and Klepaczko, 1999; Hanim and Klepaczko, 1999) as the stress level at which some dispersed micro-voids can be observed in the spall zone. If the tensile stress is lower than the incipient spall strength, no micro-voids can be visible up to a magnification of 1000X. Since spallation is a process of accumulating damage, at a given loading rate, the spall strength of a material may have a range of values corresponding to measurements of different stages of damage; hence the need for a definition of incipient spall strength. Our goal in this section is to relate our computed results on dynamic void growth to experimental measurements of incipient spall strength.

Several models have been offered for spallation. Grady (1988) proposed an energetic criterion that predicts a constant strength for ductile spall. However, experiments (Chevrier and Klepaczko, 1999; Moshe et al., 1998, 2000) show that the spall strength of a material increases as the duration of the loading pulse decreases. Johnson (1981) used Carroll and Holt's (Carroll and Holt, 1972) hollow sphere model to examine the spall strength in ductile materials. Since elasticity is omitted in this hollow sphere model, the predicted critical stress for the unstable growth of voids is raised to unrealistic levels. Curran et al. (1987) developed a model (the so-called NAG model) based on the nucleation and growth of voids. However, the exponential growth of voids in the NAG model comes from a quasi-static model of void growth, where the effects of inertia have not been included. Some other models have been described, e.g. by Hanim and Klepaczko (1999). Since the model that we have developed (in this paper and that of Wu et al. (2003)) includes the effects of elasticity, inertia, rate dependence, thermal softening and heat conduction on void growth, we seek to determine the implications for spallation. We recognize that our modeling cannot account for void–void interactions, and so we cannot address the full spallation process.

Wu et al. (2003) have shown that the growth of voids will be very limited if the applied stress is lower than the critical stress. Given the nature of ductile spall, therefore, we expect that the incipient spall strength should be higher than the critical stress that we compute for the material. Thus, the computed critical stresses should provide estimates for the incipient spall strength, and experiments that develop spall should involve supercritical loading. However, experiments (Chevrier and Klepaczko, 1999; Moshe et al., 1998, 2000) have shown that the incipient spall strength itself increases as the duration of the loading pulse is reduced. We interpret this to be a result of the fact that voids need to grow to visible sizes in order to be observed. The "equilibrium rate" of void growth under supercritical loading was determined in Eq. (24) and was shown to depend on the degree of supercriticality. Thus, for a smaller duration of loading, higher tensile stresses are needed for the voids to grow to a specific size (i.e., to be visible at a magnification of 1000X), and hence the experimental observations of the pulse duration dependence of the incipient spall strength. Once supercriticality is achieved, void growth can be extraordinarily rapid (e.g. an equilibrium growth rate of 60 μm/μs will be developed in titanium if the applied stress is only 5% higher than the critical stress). Such a calculation indicates that it will only take about a hundred nanoseconds for micro-voids to grow to visible sizes in most metals. The duration of the loading pulse in most plate impact based spallation

experiments is on the order of several hundred nanoseconds to one microsecond. This is sufficient time for voids to grow substantially according to our calculations, and thus we may again expect the lower limits of the measured spall strength to correspond to our computed critical stresses.

Measurements of the incipient (ductile) spall strengths taken from the literature are compared with our computed critical stresses in Fig. 5 for a number of the materials in Table 1 (spall data is not available on the full set of materials in Table 1). A colored or shaded rectangle is drawn around each set of data so that comparisons are easily made. In most cases, it is evident that the computed athermal critical stresses are just below the lower limits of measured spall strength (this is true for α-Ti, Ti–6Al–4V, 6061-T6 Al, tantalum and pure aluminum). In the case of annealed copper there is some overlap between the measured spall data and the computed critical stresses, and in two cases (4340 steel and 2024-T4 Al) the measured incipient spall strengths are less than the computed critical strengths. Variations in real material properties (such as strain hardening) may contribute to the large scatter of the spall strength data, but the bulk of the scatter likely arises from differences in the experimental characterization of spall strength. However, considering the difficulties associated with the experiments and the typical approximations that have to be made in both the spallation experiments and in the fitting of power-law curves to constitutive data, we believe the agreement shown in Fig. 5 is remarkably good.

Since voids grow slowly in the early stages of void growth (e.g. Fig. 7), the influence of heat conduction is substantial and near-athermal growth of the voids is a good approximation (Eq. (17)), particularly for the micro-voids that must first develop in spallation. Thus, it is reasonable to compare the lower limits of spall strength with the athermal critical stress. Once the voids begin to grow rapidly, they will grow in a near adiabatic fashion so that the adiabatic critical stress should be used in Eq. (24) to compute the equilibrium rate of void growth in this supercritical case. That is, the estimation of the spall strength should be based on the athermal critical stress but the estimation of the equilibrium rate of growth of the voids should be based on the adiabatic critical stress. Our theoretical and numerical analyses in the inertial case show the final void size not only depends on the applied load but also on the time over which the load is applied.

Many factors that might contribute to measured spall behavior are not included in our simple void growth model. We do not account for nucleation, void–void interactions, or void coalescence. Further, material properties that are necessary for the model, such as yield strength, strain hardening and thermal softening, vary strongly with material microstructure, and much of the spall literature does not provide enough microstructural information on the materials evaluated. Even when such information is available, it is possible that the large compressions associated with the loading may result in microstructural changes (including phase transformations). Further, other mechanisms than spherical void growth may be significant in the spallation of very hard materials (such as the high-strength steels). Among the materials listed in Table 1, ductile spallation has been reported in annealed copper, aluminum, titanium, etc, and brittle spallation has been reported in iron, mild steel and maraging steel. Both ductile and brittle spallation has been reported in Ti–6Al–4V (Grady, 1988). Given all of these approximations, and considering the fact that variations of 20% are considered reasonable (Grady, 1988) in spallation studies, the comparison between the observed lower limits of spall strength and the computed athermal critical stresses is certainly encouraging. It appears that we can predict the lower limits of spall strength using the approach presented here, requiring only constitutive information obtained from quasistatic experiments. Improvements in our understanding of spallation will require the inclusion of many other mechanisms, and void interactions in particular.

5. Concluding remarks

We have examined the coupled effects of thermal softening and heat conduction on the dynamic growth of a single void in an elastic–plastic medium, with a view towards addressing the dynamic failure of metals in general and spallation in particular. A brief list of our conclusions is presented below:

- The combined effects of inertia, thermal softening and heat conduction on void growth are examined. Thermal softening lowers the critical stress for unstable growth of a void and destabilizes the growth of voids. In contrast, heat conduction reduces the destabilizing effect of thermal softening.
- The dependence of the non-thermal critical stress (i.e., no thermal effects) on the yield strain of materials is shown to be a strong function of the strain hardening. Consequently the influence of the yield strain on the non-thermal critical stress tends to be significant for pure metals, but relatively insignificant for typical alloyed structural metals.
- The coupled effects of strain hardening, yield strain and thermal softening on the critical stress are computed for a number of structural metals and alloys. Both adiabatic and non-thermal critical stresses are computed; the adiabatic critical stress is 5–12% less than the non-thermal critical stress for the materials examined here. For most of the materials listed in Table 1, the critical stresses fall in the range of 1–3 GPa. Thermal softening effects are particularly pronounced for high-strength steels.
- Applied loadings that are greater than the adiabatic critical stress but less than the non-thermal critical stress (referred to as "intermediate" loadings) result in interesting phenomena strongly tied to thermal conduction. Heat conduction terminates the growth of sufficiently small voids for intermediate loadings.
- We have developed criteria (based on combinations of material properties, the void size and the void growth rate) to determine when the adiabatic void growth or the non-thermal void growth idealizations are reasonable.
- The influence of heat conduction on void growth is strongly affected by the current void size as well as the applied loading rate for the non-inertial ("quasistatic") case. Thus at high loading rates, void growth tends to be adiabatic, and unstable void growth will be essentially adiabatic.
- Thermal softening may result in a substantial increase of the rate of dynamic void growth under supercritical loading, even though it has a relatively small effect on the critical stress.
- Heat conduction effectively sets a cut-off size for the dynamic growth of a void (inertial effects included). Under supercritical loading, voids with initial sizes smaller than the cut-off size will stop growing eventually, while voids with initial sizes bigger than the cut-off size continue to grow rapidly and quickly become similar in size as a result of the equilibrium rate of growth. The influence of heat conduction on void growth is affected by the initial void sizes and the applied loading rate.
- The measured lower limits of spall strength of materials can be predicted (to an accuracy better than current experimental variations) by the computed athermal critical stress. We show that the estimation of the spall strength should be based on the athermal critical stress but the estimation of the equilibrium rate of growth of the voids should be based on the adiabatic critical stress.

Acknowledgements

This work was performed under the auspices of the Center for Advanced Metallic and Ceramic Systems (CAMCS) at Johns Hopkins. This research was sponsored by the Army Research Laboratory (ARMAC-RTP) and was accomplished under ARMAC-RTP Cooperative Agreement Number DAAD19-01-2-0003. The views and conclusions contained in this document are those of the authors and should not be interpreted as representing the official policies, either expressed or implied, of the Army Research Laboratory or the US Government. The US Government is authorized to reproduce and distribute reprints for Government purposes not withstanding any copyright notation hereon.

References

Ashby, M.F., Blunt, F.J., Bannister, M., 1989. Flow characteristics of highly constrained metal wires. Acta metall. 37, 1847–1857.
Ashby, M.F., Jones, D.R.H., 1998a. Engineering materials. Butterworth Heinemann.

Ashby, M.F., Jones, D.R.H., 1998b. Engineering materials. Butterworth Heinemann.
Ball, J.M., 1982. Discontinuous equilibrium solutions and cavitation in nonlinear elasticity. Philos. Trans. R. Soc. Lond. A 306, 557–611.
Carroll, M.M., Holt, A.C., 1972. Static and dynamic pore-collapse relations for ductile porous materials. J. Appl. Phys. 43,, 1626–1636.
Chevrier, P., Klepaczko, J.R., 1999. Spall fracture: mechanical and microstructural aspects. Engng. Fract. Mech. 63, 273–294.
Chichili, D.R., 1998. High-strain-rate deformation mechanisms and adiabatic shear localization in alpha-titanium. The Johns Hopkins University.
Cortes, R., 1992. The growth of microvoids under intense dynamic loading. Int. J. Solids Struct. 29, 1339–1350.
Cortes, R., Ellices, M., 1993. The plastic growth of a cavity nucleated at a shear band. Int. J. Solids Struct. 30, 2971–2981.
Curran, D.R., Seaman, L., Shockey, D.A., 1987. Dynamic failure of solids. Phys. Rep. 147, 253–388.
Davison, L., Graham, R.A., 1979. Shock compression of solids. Phys. Rep. 55, 255–379.
Dekel, E., Eliezer, S., Henis, Z., Moshe, E., Ludmirsky, A., Goldberg, I.B., 1998. Spallation model for the high strain rates range. J. Appl. Phys. 84, 4851–4858.
Gent, A.N., Lindley, P.B., 1958. Internal rupture of bonded rubber cylinders in tension. Proc. R. Soc. Lond. 249A, 195–205.
Grady, D.E., 1988. The spall strength of condensed matter. J. Mech. Phys. Solids 36, 353–384.
Hanim, S., Klepaczko, J.R., 1999. Numerical study of spalling in an aluminum alloy 7020-t6. Int. J. Impact Engng. 22, 649–673.
Huang, Y., Hutchinson, J.W., Tvergaard, V., 1991. Cavitation instabilities in elastic–plastic solids. J. Mech. Phys. Solids 39, 223–241.
Johnson, J.N., 1981. Dynamic fracture and spallation in ductile solids. J. Appl. Phys. 52, 2812–2825.
Meyers, M.A., 1994. Dynamic behavior of materials. John Wiley & Sons.
Moshe, E., Eliezer, S., Dekel, E., Ludmirsky, A., Henis, Z., Werdiger, M., Eliaz, N., Eliezer, D., 1998. An increase of the spall strength in aluminum, copper, and metglas at strain rates larger than 10^7 s^{-1}. J. Appl Phys. 83, 4004–4011.
Moshe, E., Eliezer, S., Henis, Z., Werdiger, M., Dekel, E., Horovitz, Y., Maman, S., Goldberg, I.B., Eliezer, D., 2000. Experimental measurements of the strength of metals approaching the theoretical limit predicted by the equation of state. Appl. Phys. Lett. 76, 1555–1557.
Ortiz, M., Molinari, A., 1992. Effect of strain hardening and rate sensitivity on the dynamic growth of a void in a plastic material. J. Appl. Mech. 59, 48–53.
Speight, C.S., Taylor, P.F., 1986. Dynamic fracture criteria from free surface velocity measurements. In: Murr, L.E., Staudhammer, K.P., Meyers, M.A. (Eds.), Metallurgical applications of shock-wave and high-strain-rate phenomena. Marcel Dekker, pp. 805–820.
Tong, W., Ravichandran, G., 1993. Dynamic pore collapse in viscoplastic materials. J. Appl. Phys. 74, 2425–2435.
Tong, W., Ravichandran, G., 1995. Inertial effects on void growth in porous viscoplastic materials. Trans. ASME: J. Appl. Mech. 62, 633–639.
Tvergaard, V., Hutchinson, J.W., 1993. Effects of initial void shape on the occurrence of cavitation instabilities in elastic–plastic solids. Trans. ASME: J. Appl. Mech. 60, 807–812.
Wu, X.Y., Ramesh, K.T., Wright, T.W., 2003. The dynamic growth of a single void in a viscoplastic material under transient hydrostatic loading. J. Mech. Phys. Solids 51, 1–26.
Zhang, S., Hsia, K.J., Pearlstein, A.J., 2002. Potential flow model of cavitation-induced interfacial fracture in a confined ductile layer. J. Mech. Phys. Solids 50, 549–569.